Disentangling random thermal motion of particles and collective expansion of source from transverse momentum spectra in high energy collisions

Hua-Rong Wei[a], Fu-Hu Liu[a,1], and Roy A. Lacey[b,2]
[a] *Institute of Theoretical Physics, Shanxi University, Taiyuan, Shanxi 030006, China*
[b] *Departments of Chemistry & Physics, Stony Brook University, Stony Brook, NY 11794, USA*

arXiv:1509.09083v3 [nucl-ex] 4 Oct 2016

Abstract: In the framework of a multisource thermal model, we describe experimental results of the transverse momentum spectra of final-state light flavour particles produced in gold-gold (Au-Au), copper-copper (Cu-Cu), lead-lead (Pb-Pb), proton-lead (p-Pb), and proton-proton (p-p) collisions at various energies, measured by the PHENIX, STAR, ALICE, and CMS Collaborations, by using the Tsallis-standard (Tsallis form of Fermi-Dirac or Bose-Einstein), Tsallis, and two- or three-component standard distributions which can be in fact regarded as different types of "thermometers" or "thermometric scales" and "speedometers". A central parameter in the three distributions is the effective temperature which contains information on the kinetic freeze-out temperature of the emitting source and reflects the effects of random thermal motion of particles as well as collective expansion of the source. To disentangle both effects, we extract the kinetic freeze-out temperature from the intercept of the effective temperature (T) curve as a function of particle's rest mass (m_0) when plotting T versus m_0, and the mean transverse flow velocity from the slope of the mean transverse momentum ($\langle p_T\rangle$) curve as a function of mean moving mass ($\overline{m}$) when plotting $\langle p_T\rangle$ versus $\overline{m}$.

Keywords: Kinetic freeze-out temperature, Transverse flow velocity, Transverse momentum spectrum, Tsallis-standard distribution, Tsallis distribution, Standard distribution

PACS: 25.75.-q, 25.75.Ag, 25.75.Ld

1 Introduction

Comparing with fixed target experiments, the Relativistic Heavy Ion Collider (RHIC) in the USA and the Large Hadron Collider (LHC) in Switzerland attract more studies due to their exhibitions on the evolution process of interacting system in collisions at higher energies. The experiments at RHIC and LHC are more complex and difficult for some limited conditions, which render very limited measurable quantities. It is expected that more interacting information can be extracted from these limited measurable quantities. For example, by analyzing the transverse momentum spectra of final-state particles, one can obtain the kinetic freeze-out temperature of interacting systems (emission sources) and the transverse flow velocity of produced particles. These two quantities reflect the excited degree of emission sources and hydrodynamic expansion picture of interacting systems at the stage of kinetic freeze-out, when hadrons are no longer interactive and their momenta do not change [1].

In high energy collisions, one can use different distribution laws to describe the transverse momentum spectra of final-state particles. In the framework of a multisource thermal or statistical model, we can use the standard (Boltzmann, Fermi-Dirac, or Bose-Einstein) distribution [2], the multi-component standard distribution, the Tsallis distribution (statistics), the Tsallis-standard (Tsallis forms of the standard) distribution [3], the Erlang distribution, the multi-component Erlang distribution [4], the Lévy distribution [5, 6], the blast-wave function [7], the power law, and so forth, to describe the particle transverse momentum spectrum contributed by a given emission source. From the distributions mentioned above, one can directly extract the effective temperature, which is actually not the real temperature (kinetic freeze-out temperature) of the emission source. The real temperature of the emission source should reflect purely thermal motion of particles in the source, while the effective temperature extracted from the transverse momentum spectrum includes both thermal motion and flow effect of particles, and is greater than the

[1] E-mail: fuhuliu@163.com; fuhuliu@sxu.edu.cn
[2] E-mail: Roy.Lacey@Stonybrook.edu

real temperature. Only if the effect of flow is excluded in the extraction of source temperature, can we obtain the kinetic freeze-out temperature.

In this paper, within the framework of the multisource thermal model [8–10], we use the Tsallis-standard distribution, Tsallis distribution, and two- or three-component standard distribution [3] to describe the transverse momentum spectra of final-state light flavour particles produced in gold-gold (Au-Au), copper-copper (Cu-Cu), lead-lead (Pb-Pb), proton-lead (p-Pb), and proton-proton (p-p) collisions with different centrality intervals over a center-of-mass energy ($\sqrt{s_{NN}}$) range from 0.2 to 7 TeV. Although we can obtain the analytical expressions for the mentioned distributions, the Monte Carlo method is used to see the statistical fluctuations in the process of calculation. The results from the Monte Carlo method are compared with the experimental data of the PHENIX [11], STAR [12], ALICE [13–18], and CMS Collaborations [19]. The kinetic freeze-out temperature of interacting system and transverse flow velocity of final-state particles are then extracted from the comparisons and analyses.

2 The model and formulism

In this paper, the transverse momentum spectra are described in the framework of the multisource thermal model [8–10], which assumes that many emission sources are formed in high energy collisions and are separated into a few groups resulting from different interacting mechanisms in the collisions as well as different event samples in experiment measurements. The sources in the same group have the same excitation degree and stay at a common local equilibrium state, which can be described by using different distribution laws. The final-state distribution is attributed to all sources in different groups, which results in a multi-temperature emission process if we use the standard distribution. This also means that the transverse momentum spectra can be described by a multi-component standard distribution which can be fitted by the Tsallis distribution. In fact, we can adopt one-component Tsallis-standard (T-S) distribution (Tsallis form of the Boltzmann, Fermi-Dirac, or Bose-Einstein distribution), one-component Tsallis distribution, and two- or three-component standard distribution (Boltzmann, Fermi-Dirac, or Bose-Einstein distribution), to describe the transverse momentum spectra of final-state light flavour particles.

According to refs. [3, 20], we use the uniform expressions of the Tsallis-standard distribution and Tsallis distribution which have more than one version [20–26], respectively. Based on the invariant particle momentum distribution, as well as the unit-density function of transverse momentum (p_T) and rapidity (y), the Tsallis-standard transverse momentum distribution and the Tsallis transverse momentum distribution are derived [3, 20]. In the present work, the formalism of the Tsallis-standard transverse momentum distribution is adopted to be [3, 20]

$$f_{\text{T-S}}(p_T)=\frac{1}{N}\frac{dN}{dp_T}=C_{\text{T-S0}}p_T\sqrt{p_T^2+m_0^2}\int_{y_{\min}}^{y_{\max}}\cosh y\left\{\left[1\pm\frac{q_{\text{T-S}}-1}{T_{\text{T-S}}}\left(\sqrt{p_T^2+m_0^2}\cosh y-\mu\right)\right]^{\pm\frac{1}{q_{\text{T-S}}-1}}+S\right\}^{-1}dy, \tag{1}$$

where $C_{\text{T-S0}}$ is the normalization constant $gV/(2\pi)^2$ which results from $\int_0^\infty f_{\text{T-S}}(p_T)dp_T=1$; g, V, N, μ, and m_0 are degeneracy factor, volume, particle number, chemical potential, and particle's rest mass, respectively; $y_{\min}$ is the minimum rapidity and $y_{\max}$ is the maximum rapidity; The + and − in the ± sign are for $\sqrt{p_T^2+m_0^2}\cosh y>\mu$ and $\sqrt{p_T^2+m_0^2}\cosh y\le\mu$, respectively; S has values 0, +1, and −1, which denote the Boltzmann, Fermi-Dirac, and Bose-Einstein distributions, respectively; $T_{\text{T-S}}$ is the effective temperature of emission sources and $q_{\text{T-S}}$ is the entropy index or nonequilibrium degree factor.

In the calculation, since the effect of chemical potential can be ignored (i.e. $\mu=0$) in collisions at RHIC and LHC energies, we have $\sqrt{p_T^2+m_0^2}\cosh y>\mu$ and take + in the ± sign. The final Tsallis-standard p_T distribution is given by

$$f_{\text{T-S}}(p_T)=\frac{1}{N}\frac{dN}{dp_T}=C_{\text{T-S0}}p_T\sqrt{p_T^2+m_0^2}\int_{y_{\min}}^{y_{\max}}\cosh y\left\{\left[1+\frac{q_{\text{T-S}}-1}{T_{\text{T-S}}}\sqrt{p_T^2+m_0^2}\cosh y\right]^{\frac{1}{q_{\text{T-S}}-1}}+S\right\}^{-1}dy. \tag{2}$$

Further, considering $S=0$ and the power index $q_{\text{T-S}}/(q_{\text{T-S}}-1)$ and other limitations, the Tsallis transverse momentum distribution is obtained and can be written as [20]

$$f_{\text{T}}(p_T)=\frac{1}{N}\frac{dN}{dp_T}=C_{\text{T0}}p_T\sqrt{p_T^2+m_0^2}\int_{y_{\min}}^{y_{\max}}\cosh y\left[1+\frac{q_{\text{T}}-1}{T_{\text{T}}}\sqrt{p_T^2+m_0^2}\cosh y\right]^{-\frac{q_{\text{T}}}{q_{\text{T}}-1}}dy, \tag{3}$$

where $C_{\rm T0}$ is the normalization constant which gives $\int_0^\infty f_{\rm T}(p_T)dp_T = 1$, $T_{\rm T}$ is the effective temperature, and $q_{\rm T}$ is the entropy index or nonequilibrium degree factor. Sometimes the upper index $q_{\rm T}/(q_{\rm T}-1)$ is replaced by $1/(q_{\rm T}-1)$ due to $q_{\rm T}$ being very close to 1 and application of mean field approximation. The latter obtains a smaller $q_{\rm T}$.

Particularly, in the present work, we also use the two- or three-component standard distribution, which is different from the distributions introduced above. The standard Boltzmann, Fermi-Dirac, and Bose-Einstein distributions for the ith component (group) can be uniformly shown as

$$f_i(p_T) = \frac{1}{N}\frac{dN}{dp_T} = C_{i0}p_T\sqrt{p_T^2+m_0^2}\int_{y_{\rm min}}^{y_{\rm max}}\cosh y\left[\exp\left(\frac{\sqrt{p_T^2+m_0^2}\cosh y}{T_i}\right)+S\right]^{-1}dy, \tag{4}$$

where C_{i0} is the normalization constant which gives $\int_0^\infty f_i(p_T)dp_T = 1$ and T_i is the effective temperature for the ith component. In final state, the p_T spectrum is contributed by the l components of the distribution; that is

$$f_{\rm S}(p_T) = \frac{1}{N}\frac{dN}{dp_T} = \sum_{i=1}^{l} k_i f_i(p_T), \tag{5}$$

where k_i is the relative weight contributed by the ith component. This is the multi-component standard distribution. Considering the relative contribution of each component, we have the mean effective temperature to be

$$T_{\rm S} = \sum_{i=1}^{l} k_i T_i, \tag{6}$$

where $T_{\rm S}$ reflects the mean excitation degree for different components and can be used to describe the effective temperature of emission source. We would like to point out that Eq. (6) is not a simple additive treatment for different temperatures, but an average weighted by different k_i, where $\sum_{i=1}^{l} k_i = 1$.

It is expected that we can obtain the relation between the effective temperature T ($T_{\rm T\text{-}S}$, $T_{\rm T}$, or $T_{\rm S}$) and the particle's rest mass m_0. A linear fitting can obtain the intercept T_0 ($T_{\rm T\text{-}S0}$, $T_{\rm T0}$, or $T_{\rm S0}$) in linear relation $T - m_0$. As the temperature corresponds to massless ($m_0 = 0$) particle, T_0 is regarded as the source real temperature, or the kinetic freeze-out temperature of interacting system. According to refs. [11, 27–30], we have the relation between T and T_0,

$$T = T_0 + am_0. \tag{7}$$

According to refs. [27, 28], the slope a can be given by $v_0^2/2$ and v_0 is the (average and transverse) radial flow velocity which is valid for low p_T only. Considering different distribution laws, v_0 can be $v_{\rm T\text{-}S0}$, $v_{\rm T0}$, or $v_{\rm S0}$, and T_0 can be $T_{\rm T\text{-}S0}$, $T_{\rm T0}$, or $T_{\rm S0}$, corresponding to Tsallis-standard, Tsallis, or standard distribution, respectively. In the above discussions, different distribution laws are in fact regarded as different types of "thermometers" or "thermometric scale" and "speedometers".

Since $a = v_0^2/2$ in Eq. (7) is only valid for low p_T region [27, 28], whereas the effective temperature is extracted in the present work for fits in p_T range which goes beyond 2 GeV/c, we give up to extract radial flow v_0 from the slope a in Eq. (7). Although other works [11, 29, 30] also regard the intercept T_0 in Eq. (7) as the kinetic freeze-out temperature, different relations between radial flow velocity v_0 and slope a are used, and in some cases the relation is undetermined. In view of uncertain relations between radial flow velocity and slope in wide p_T range, we give up to extract radial flow velocity from the slope, and extract only the kinetic freeze-out temperature from T_0 in Eq. (7).

We need an alternative method to extract mean (transverse) flow velocity. In our very recent work [31], the linear relations between T and m_0 [Eq. (7)], mean transverse momentum $\langle p_T\rangle$ and m_0, mean momentum $\langle p\rangle$ and m_0, T and mean moving mass $\overline{m}$, $\langle p_T\rangle$ and $\overline{m}$, as well as $\langle p\rangle$ and $\overline{m}$ are studied. From the analyses on dimension and quantity, we regard the intercept in $T - m_0$ relation [Eq. (7)] as the kinetic freeze-out temperature and the slope in $\langle p_T\rangle - \overline{m}$ (or $\langle p\rangle - \overline{m}$) relation as the mean transverse flow velocity $\langle u_T\rangle$ (or mean flow velocity $\langle u\rangle$). Particularly, for $\langle p_T\rangle - \overline{m}$ and $\langle p\rangle - \overline{m}$ relations, we have

$$\langle p_T\rangle = \langle p_T\rangle_0 + \langle u_T\rangle\overline{m} \tag{8}$$

and

$$\langle p\rangle = \langle p\rangle_0 + \langle u\rangle\overline{m}, \tag{9}$$

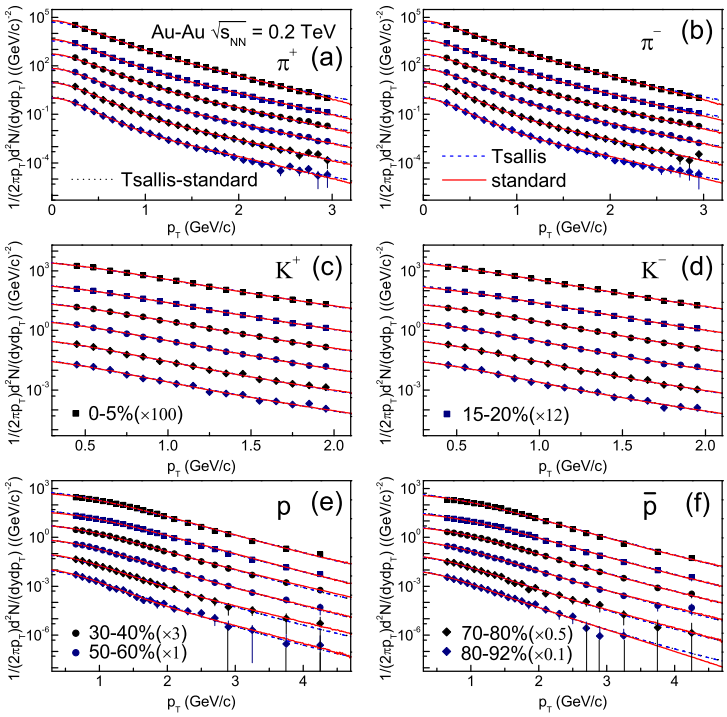

Figure 1. Transverse momentum spectra for (a) π^+, (b) π^-, (c) K^+, (d) K^-, (e) p, and (f) $\bar{p}$ produced in Au-Au collisions with different centrality bins at $\sqrt{s_{NN}} = 0.2$ TeV. The data are measured by the PHENIX Collaboration at midrapidity [11] and are scaled vertically as quoted in the figure. The dotted, dashed, and solid curves are our results calculated by using the Tsallis-standard, Tsallis, and two-component standard distributions, respectively.

where $\langle p_T\rangle_0$ and $\langle p\rangle_0$ denote the mean transverse momentum and mean momentum of massless particle, respectively. We would like to point out that, in the case of describing meanwhile the same experimental data, the three distributions result in nearly the same $\langle p_T\rangle$ (or $\langle p\rangle$), the same $\langle p_T\rangle - \overline{m}$ (or $\langle p\rangle - \overline{m}$) relation, and the same $\langle u_T\rangle$ (or $\langle u\rangle$).

From the above analyses, we see that the linear relations between T and m_0, $\langle p_T\rangle$ and $\overline{m}$, as well as $\langle p\rangle$ and $\overline{m}$ [Eqs. (7)–(9)] can be respectively obtained from the same set of parameter values which are extracted from the same set of experimental data. This means that the extraction processes of T_0, $\langle u_T\rangle$, and $\langle u\rangle$ are independent, though their values are entangled due to the same set of parameters. In particular, v_0 and the slope in Eq. (7) are related to (transverse) flow velocity. However, there is no obvious and exact relation between them [11, 27–30]. Anyhow, we think that the intercept in Eq. (7), the slope in Eq. (8), and the slope in Eq. (9) can provide a set of alternative methods to extract the kinetic freeze-out temperature, transverse flow velocity, and flow velocity, respectively [31]. Thus, we can use this set of alternative methods in the present work to extract separately the kinetic freeze-out temperature and transverse flow velocity according to transverse momentum spectra. This set of alternative methods is also used to judge different kinetic freeze-out scenarios in our another recent work [32] in which an evidence of mass-dependent differential kinetic freeze-out scenario is observed, while the single and double kinetic freeze-out scenarios are eliminated.

3 Results and discussion

Figure 1 presents the centrality dependence of p_T spectra for (a) π^+, (b) π^-, (c) K^+, (d) K^-,

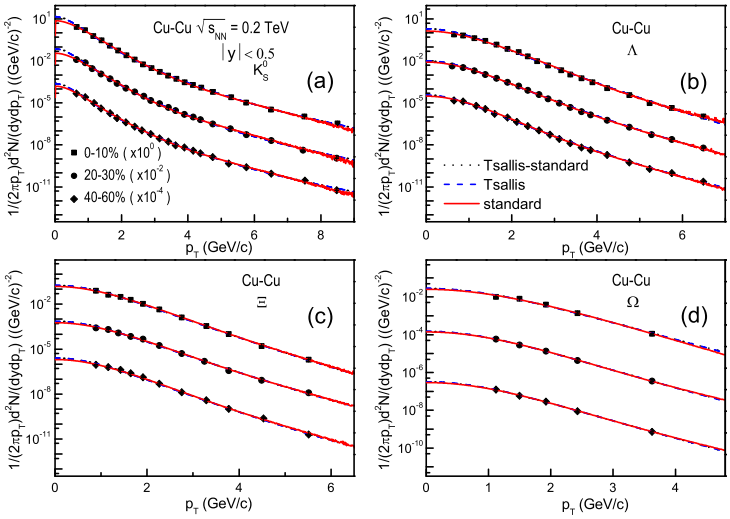

Figure 2. Transverse momentum spectra of (a) K^0_S, (b) Λ, (c) Ξ, and (d) Ω produced in Cu-Cu collisions at $\sqrt{s_{NN}} = 0.2$ TeV in three centrality intervals. The symbols represent the experimental data recorded by the STAR Collaboration in the rapidiy range $|y| < 0.5$ [12]. The dotted, dashed, and solid curves are our results calculated by using the Tsallis-standard, Tsallis, and two- or three-component standard distributions, respectively.

(e) p, and (f) $\bar{p}$ produced in Au-Au collisions at center-of-mass energy $\sqrt{s_{NN}} = 0.2$ TeV. The data measured by the PHENIX Collaboration at midrapidity [11] are represented by different symbols which correspond to different centrality (C) bins from 0–5% to 80–92% scaled by different amounts as shown in the panels for clarity. The error bars are statistical only. The dotted, dashed, and solid curves are our results calculated by using the Tsallis-standard, Tsallis, and two-component standard distributions, respectively. The values of free parameters ($T_{\rm T\text{-}S}$, $q_{\rm T\text{-}S}$, $T_{\rm T}$, and $q_{\rm T}$), normalization constants ($N_{\rm T\text{-}S0}$ and $N_{\rm T0}$) for comparisons between curves and data, and χ^2 per degree of freedom (χ^2/dof) for Tsallis-standard and Tsallis distributions are given in Table 1. The values of free parameters (T_1, k_1, and T_2), mean effective temperature ($T_{\rm S}$), normalization constant ($N_{\rm S0}$) for comparisons between curves and data, and χ^2/dof for two-component standard distribution are listed in Table 2. One can see that all three types of distribution laws are consistent with the experimental data. The effective temperatures $T_{\rm T\text{-}S}$, $T_{\rm T}$, and $T_{\rm S}$ increase with the increase of centrality or particle mass, and $T_{\rm T\text{-}S} \leq T_{\rm T} < T_{\rm S}$ for a given set of data. We would like to point out that the increase of centrality and the decrease of centrality percentage have the same meaning.

Figure 2 shows p_T spectra of (a) K^0_S, (b) Λ, (c) Ξ, and (d) Ω produced in Cu-Cu collisions at $\sqrt{s_{NN}} = 0.2$ TeV in different centrality intervals of 0–10%, 20–30%, and 40–60%. The symbols represent the experimental data recorded by the STAR Collaboration in the rapidiy range $|y| < 0.5$ [12]. For clarity, the results for different C intervals are scaled by different amounts shown in the panels. The uncertainties on the data points include both statistical and systematic errors. The dotted, dashed, and solid curves are our results based on the Tsallis-standard, Tsallis, and two- or three-component standard transverse momentum distributions, respectively. The values of free parameters ($T_{\rm T\text{-}S}$, $q_{\rm T\text{-}S}$, $T_{\rm T}$, $q_{\rm T}$, T_1, k_1, T_2, k_2, and T_3), $T_{\rm S}$, normalization constants ($N_{\rm T\text{-}S0}$, $N_{\rm T0}$, and $N_{\rm S0}$), and χ^2/dof are displayed in Tables 1 and 2. Obviously, the experimental data can be described by the three types of fit functions for p_T in all centrality bins. The effective temperatures $T_{\rm T\text{-}S}$, $T_{\rm T}$, and $T_{\rm S}$ increase with the increase of centrality or particle mass, and $T_{\rm T\text{-}S} \leq T_{\rm T} < T_{\rm S}$ for a given set of data.

The p_T spectra of (a) π^+, (b) K^+, (c) p, and (d) ϕ produced in central (0–5%), semi-central (50–60%), and peripheral (80–90%) Pb-Pb collisions at $\sqrt{s_{NN}} = 2.76$ TeV are displayed in Fig. 3, where $N_{\rm ev}$ denotes the number of events. The data points are measured by the ALICE Collaboration at midrapidity ($|y| < 0.5$) [13, 14]. The error bars combined both statistical and systematic uncertainties. The fitting

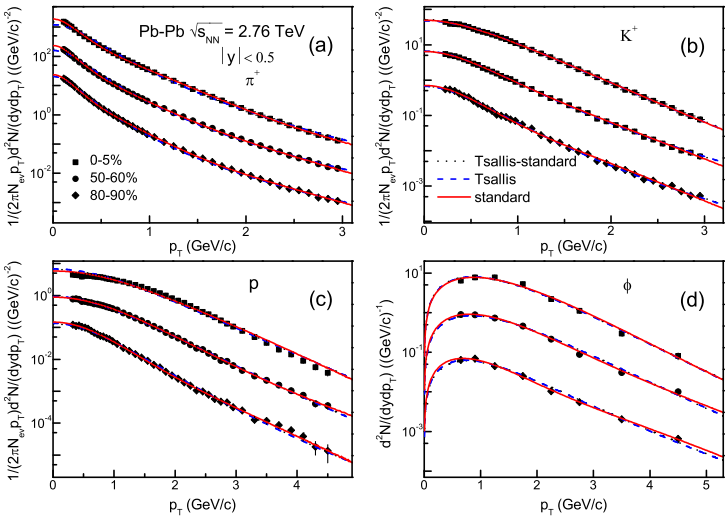

Figure 3. Transverse momentum spectra of (a) π^+, (b) K^+, (c) p, and (d) ϕ produced in Pb-Pb collisions at $\sqrt{s_{NN}} = 2.76$ TeV in three centrality intervals. The symbols represent the experimental data measured by the ALICE Collaboration at mid-rapidity ($|y| < 0.5$) [13, 14]. The fitting results with three types of distributions are plotted by the curves.

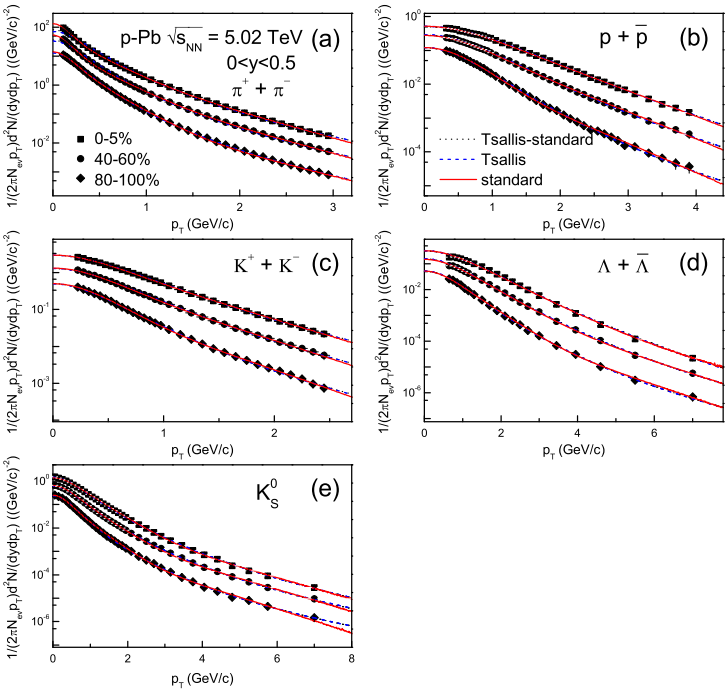

Figure 4. Transverse momentum spectra of (a) $\pi^{\pm}$, (b) $p + \bar{p}$, (c) $K^{\pm}$, (d) $\Lambda + \bar{\Lambda}$, and (e) K^0_S in p-Pb collisions in different centrality classes at $\sqrt{s_{NN}} = 5.02$ TeV. The experimental data represented by the symbols are performed by the ALICE Collaboration in $0 < y < 0.5$ [15]. Our fitting results are exhibited by the curves.

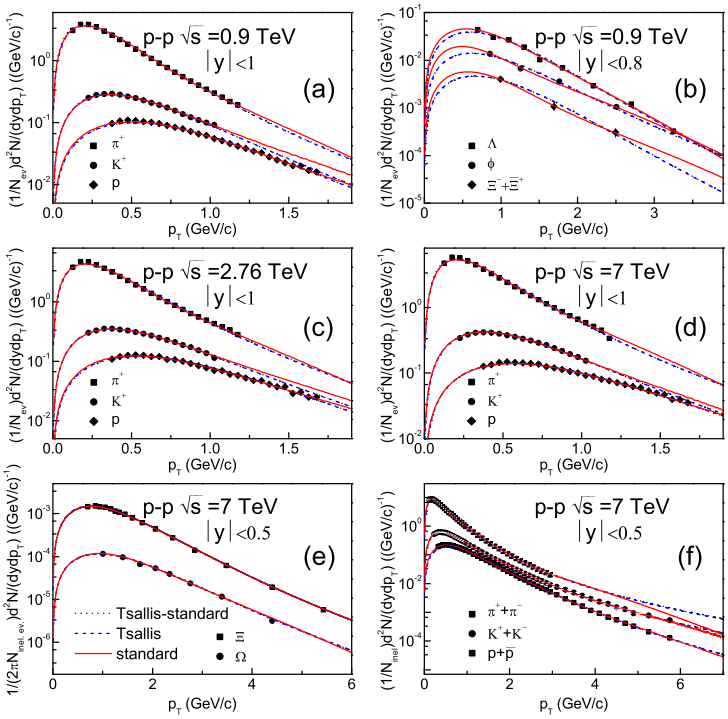

Figure 5. Transverse momentum spectra of various identified hadrons produced in p-p collisions. The symbols in Figs. 5(a), 5(c), and 5(d) represent the experimental data for π^+, K^+, and p measured by the CMS Collaboration [19] in the range $|y| < 1$ at $\sqrt{s} = 0.9, 2.76, 7$ TeV, respectively. The data points of the ALICE Collaboration measured in $|y| < 0.8$ at $\sqrt{s} = 0.9$ TeV for Λ, ϕ, and $\Xi^- + \bar{\Xi}^+$ [16], in $|y| < 0.5$ at $\sqrt{s} = 7$ TeV for Ξ and Ω [17], and in $|y| < 0.5$ at $\sqrt{s} = 7$ TeV for $\pi^{\pm}$, $K^{\pm}$, and p+$\bar{p}$ [18] are shown in Figs. 5(b), 5(e), and 5(f), respectively. The fitting curves are our results.

results with Tsallis-standard, Tsallis, and two- or three-component standard distributions are plotted by the dotted, dashed, and solid curves, respectively. The values of free parameters, $T_{\rm S}$, normalization constants, and χ^2/dof are shown in Tables 1 and 2. These fitting functions describe the experimental data. Once again, the effective temperatures $T_{\rm T\text{-}S}$, $T_{\rm T}$, and $T_{\rm S}$ increase with increase of centrality or particle mass, and $T_{\rm T\text{-}S} \leq T_{\rm T} < T_{\rm S}$ for a given set of data.

Figure 4 exhibits p_T spectra of (a) $\pi^{\pm}$, (b) $p + \bar{p}$, (c) $K^{\pm}$, (d) $\Lambda + \bar{\Lambda}$, and (e) K^0_S produced in p-Pb collisions in different centrality classes (0–5%, 40–60%, and 80–100%) at $\sqrt{s_{NN}} = 5.02$ TeV. The experimental data represented by different symbols are performed by the ALICE Collaboration in the rapidity interval $0 < y < 0.5$ [15]. The statistical and systematic uncertainties are combined in the error bars. Our results from the analyses of the Tsallis-standard, Tsallis, and two- or three-component standard distributions are exhibited by the dotted, dashed, and solid curves, respectively. The values of free parameters, T_S, normalization constants, and χ^2/dof are summarized in Tables 1 and 2. As can be seen, the fitting results are in agreement with the experimental data. The effective temperatures $T_{\rm T\text{-}S}$, $T_{\rm T}$, and $T_{\rm S}$ increase with the increase of centrality or particle mass, and $T_{\rm T\text{-}S} \leq T_{\rm T} < T_{\rm S}$ for a given set of data.

Figure 5 gives p_T spectra of various identified hadrons produced in p-p collisions at different energies, where $N_{\rm inel}$ denotes the number of inelastic events. The symbols in Figs. 5(a), 5(c), and 5(d) represent the experimental data for π^+, K^+, and p measured by the CMS Collaboration [19] in the range $|y| < 1$ at $\sqrt{s} = 0.9$, 2.76, and 7 TeV, respectively. The data points of the ALICE Collaboration measured in $|y| < 0.8$ at $\sqrt{s} = 0.9$ TeV for Λ, ϕ, and $\Xi^- + \bar{\Xi}^+$ [16], in $|y| < 0.5$ at $\sqrt{s} = 7$ TeV for Ξ and Ω [17], and in $|y| < 0.5$ at $\sqrt{s} = 7$ TeV for $\pi^{\pm}$, $K^{\pm}$, and p+$\bar{p}$ [18] are shown in Figs. 5(b), 5(e), and

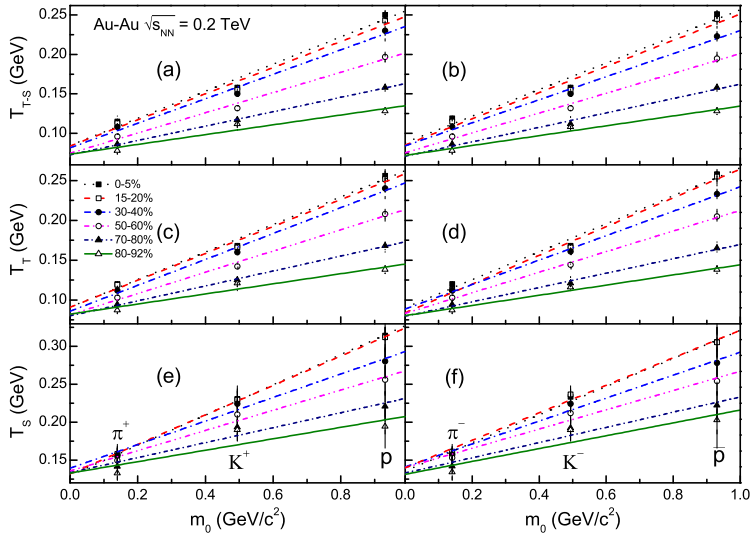

Figure 6. Particle mass and centrality dependences of $T_{\rm T\text{-}S}$, $T_{\rm T}$, and $T_{\rm S}$ for positive [left: (a), (c), and (e)] and negative particles [right: (b), (d), and (f)] in Au-Au collisions at $\sqrt{s_{NN}} = 0.2$ TeV. The symbols represent the parameter values extracted from Fig. 1 and listed in Tables 1 and 2. The lines represent linear fits to the results from each centrality bin as a function of mass using Eq. (7).

5(f), respectively. The uncertainties corresponding to combined statistics and systematics are shown as error bars. The fitting results (dotted, dashed, and solid curves) using mentioned functional forms (Tsallis-standard, Tsallis, and two- or three-component standard distributions) are superimposed. The values of free parameters, T_S, normalization constants, and χ^2/dof are exhibited in Tables 1 and 2. Once more, the Tsallis-standard, Tsallis, and two- or three-component standard distributions can describe the experimental data of the considered particles. The effective temperatures $T_{\rm T\text{-}S}$, $T_{\rm T}$, and $T_{\rm S}$ increase with the increase of particle mass, and $T_{\rm T\text{-}S} \leq T_{\rm T} < T_{\rm S}$ for a given set of data.

To see clearly the dependences of effective temperatures $T_{\rm T\text{-}S}$, $T_{\rm T}$, and $T_{\rm S}$ on centrality and particle mass, the related values listed in Tables 1 and 2, which are extracted from figures 1, 2, 3, and 4, are analyzed in Figs. 6, 7, 8 (left panel), and 8 (right panel), respectively. Different symbols correspond to different centrality intervals shown in the panels. The lines are our fitted results. At the same time, Fig. 9 shows the dependences of effective temperatures on particle mass for p-p collisions at the LHC energies. Different symbols correspond to different effective temperatures which are listed in Tables 1 and 2 and extracted from Fig. 5. The lines are our fitted results. Conclusions obtained from Figs. 1–5 and Tables 1 and 2 can be clearly seen from Figs. 6–9.

In Figs. 6–9, the lines are worthwhile for further investigation. In fact, according to Eq. (7), the intercepts at $m_0 = 0$ are real temperatures (kinetic freeze-out temperatures) $T_{\rm T\text{-}S0}$, $T_{\rm T0}$, and $T_{\rm S0}$, which are extracted from Tsallis-standard, Tsallis, and two- or three-component standard distributions, respectively. We show the dependences of kinetic freeze-out temperatures on centrality C and energy $\sqrt{s_{NN}}$ in Fig. 10 for different sizes of collisions, where the related values for p-p collisions are compared with central (0–5%) nucleus-nucleus collisions. In most cases, $T_{\rm T\text{-}S0} \leq T_{\rm T0} < T_{\rm S0}$. The kinetic freeze-out temperatures decrease slightly with the decrease of centrality (or with increase of centrality percentage), and do not show an obvious change with energy and size for the central, semi-central, and peripheral collisions. In the considered energy range from 0.2 to 7 TeV, the mean kinetic freeze-out temperatures ($\langle ... \rangle$) extracted from different distribution laws for the mentioned three centralities are marked in the panels by the specific values and dashed lines. We see that $\langle T_{\rm T\text{-}S0} \rangle \leq \langle T_{\rm T0} \rangle < \langle T_{\rm S0} \rangle$, and $\langle T_0 \rangle_{\rm central} > \langle T_0 \rangle_{\rm semi\text{-}central} \geq \langle T_0 \rangle_{\rm peripheral}$. The independences of kinetic freeze-out temperatures on energy and size render that different interacting systems at the stage of kinetic freeze-out reached the same excitation degree of hadronic matter in the considered energy range.

We noticed that the value of kinetic freeze-out temperature $T_{\rm S0}$ [(156 ± 6) MeV] in central collisions

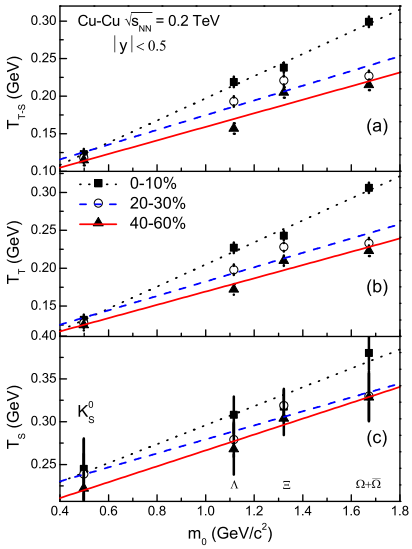

Figure 7. Same as Fig. 6, but for dependences of (a) $T_{\mathrm{T\text{-}S}}$, (b) T_{T}, and (c) T_{S} on particle mass and centrality in Cu-Cu collisions at $\sqrt{s_{NN}} = 0.2$ TeV. The symbols represent the parameter values extracted from Fig. 2.

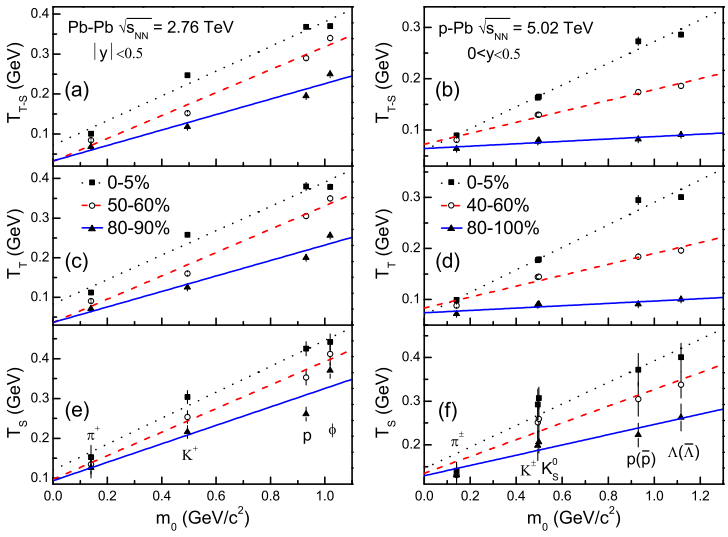

Figure 8. Same as Fig. 6, but for particle mass and centrality dependences of $T_{\mathrm{T\text{-}S}}$, T_{T}, and T_{S} for particles in Pb-Pb collisions at $\sqrt{s_{NN}} = 2.76$ TeV [left: (a), (c), and (e)], and in p-Pb collisions at $\sqrt{s_{NN}} = 5.02$ TeV [right: (b), (d), and (f)]. The symbols represent the parameter values extracted from Figs. 3 and 4.

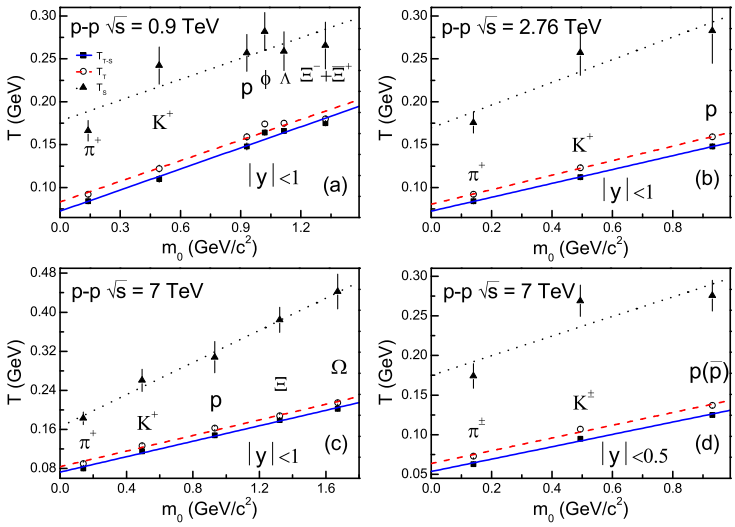

Figure 9. Same as Fig. 6, but for dependences of $T_{\rm T\text{-}S}$, $T_{\rm T}$, and $T_{\rm S}$ on particle mass in p-p collisions at (a) $\sqrt{s}$ = 0.9 TeV, (b) $\sqrt{s}$ = 2.76 TeV, (c) $\sqrt{s}$ = 7 TeV for positive particles, and (d) $\sqrt{s}$ = 7 TeV for charged particles. The symbols represent the parameter values extracted from Fig. 5.

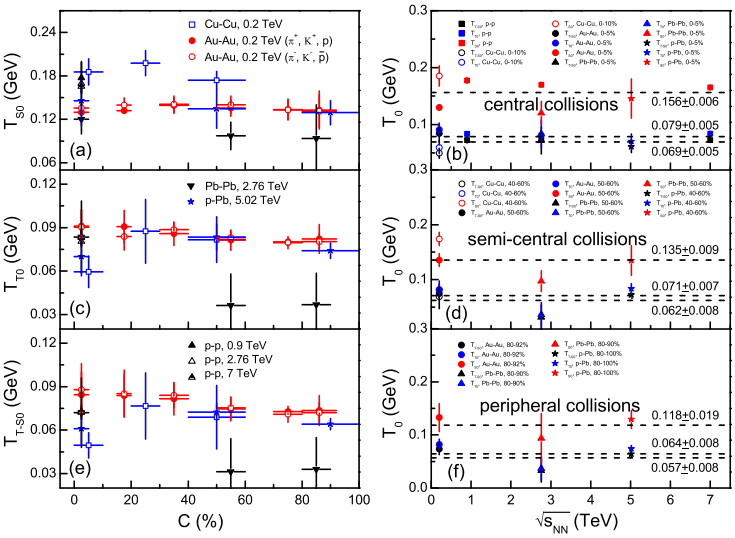

Figure 10. Centrality, energy, and size dependences of kinetic freeze-out temperatures $T_{\rm T\text{-}S0}$, $T_{\rm T0}$, and $T_{\rm S0}$. The left panel [(a), (c), and (e)] is mainly for different kinetic freeze-out temperatures and centralities, and the right panel [(b), (d), and (f)] is mainly for three centralities and different energies. The symbols represent our fitted results from Figs. 6–9. The results for p-p collisions are plotted for comparisons with central (0–5%) nucleus-nucleus collisions. The dashed lines marked with specific values in the right panel represent the three averages $\langle T_{\rm T\text{-}S0}\rangle$, $\langle T_{\rm T0}\rangle$, and $\langle T_{\rm S0}\rangle$ for three centralities, where $\langle T_{\rm T\text{-}S0}\rangle \leq \langle T_{\rm T0}\rangle < \langle T_{\rm S0}\rangle$.

[Fig. 10(b)] is less than that of chemical freeze-out temperature (170 MeV) used in some theoretical estimations for the critical point of QCD (quantum chromodynamics) [33–35]. Our result is also less than that of kinetic freeze-out temperature (177 MeV) extracted from an exponential shape of transverse mass spectrum [11], and equal to that of chemical freeze-out temperature (156 MeV) extracted from particle ratios in a thermal and statistical model [36]. The latter item means that the kinetic freeze-out temperature obtained in the present work is greater than that obtained from the thermal and statistical model [36], or the kinetic and chemical freeze-outs had happened at almost the same time. We are inclined to the latter. These results are not exactly consistent with each other even if we consider the kinetic freeze-out temperature being less than the chemical freeze-out temperature. It is undoubted that more analyses are needed in the future.

To extract the transverse flow velocity, we analyze $\langle p_T\rangle - \overline{m}$ relations in Fig. 11, where the related parameters listed in Tables 1 and 2 are used to calculate $\langle p_T\rangle$ and $\overline{m}$, where the three distributions result in the same relations. Different symbols correspond to different centrality intervals shown in the panels. The lines are our fitted results. From the slopes, we can obtain the mean transverse flow velocities of particles produced in collisions with different centralities and at different energies. The related results are shown in Figs. 12(a) and 12(b) respectively, where the results for p-p collisions are shown at $C = 2.5\%$ for comparisons. One can see that the mean transverse flow velocity in central collisions is greater than that in peripheral collisions. The relative difference is about 10%.

The mean transverse flow velocity $\langle u_T\rangle$ $[(0.443 \pm 0.071)c]$ for central collisions obtained in the present work is comparable with the radial flow velocity $[(0.426 - 0.472)c]$ [37, 38] of the blast-wave model [7, 37, 38], while the value of $\langle u_T\rangle$ $[(0.403 \pm 0.079)c]$ for peripheral collisions obtained in the present work is far from the radial flow velocity (≈ 0) [37] of the blast-wave model [7, 37, 38]. In fact, $\langle u_T\rangle$ contains isotropic radial flow and anisotropic collective flow (directed flow and others). In central collisions, the effect of anisotropic collective flow is small [39], $\langle u_T\rangle$ contains mainly the isotropic radial flow. In peripheral collisions, the isotropic radial flow is nearly zero [37], $\langle u_T\rangle$ contains mainly the anisotropic collective flow [39]. According to Fig. 12(b), $\langle u_T\rangle$ in central collisions (which contains mainly the isotropic radial flow) is greater than that in peripheral collisions (which contains mainly the anisotropic collective flow).

Because of $\langle u_T\rangle$ containing the isotropic radial flow and anisotropic collective flow together, it is different from the original blast-wave model [7, 37, 38] in which only the isotropic radial flow is contained. Our explanation on flow components is comparable with the improved blast-wave model [40, 41, 42] in which the third parameter is introduced to describe the anisotropic transverse flow generated in non-central collisions [40] and the fourth parameter is introduced to take into account the anisotropic shape of the source in coordinate space [41]. Although the dependence of elliptic flow on transverse momentum is described, the velocity of anisotropic transverse flow is not available in the improved blast-wave model [40, 41, 42]. As an indirect measurement of model independence, the present work is hoped to cause a further discussion on the flow velocity.

The kinetic freeze-out temperature and transverse flow velocity are extracted from the transverse momentum spectra, though the methodology used in the present work is different from that of the blast-wave model with the Boltzmann-Gibbs distribution or the Tsallis statistics [7, 37, 38], or the quark recombination model with the Cooper-Frye formula and flow [43]. In the latter two models, the kinetic freeze-out temperature and radial flow velocity can be obtained from certain formula description. In the present work, we obtain the effective temperature from the formula of transverse momentum distribution, and kinetic freeze-out temperature from the intercept in linear $T - m_0$ relation [Eq. (7)] [11, 27, 29–32] and the transverse flow velocity from the slope in linear $\langle p_T\rangle - \overline{m}$ relation [Eq. (8)] [32]. The method used in the present work needs two steps to obtain the kinetic freeze-out temperature and transverse flow velocity, though the process of calculation is simple.

Although the topic discussed by us was intensively discussed in the literature and similar fitting and discussion were carried out in the literature many times, we have used an alternative methodology [11, 27, 29–32] to extract the kinetic freeze-out temperature and transverse flow velocity, and the analysis is more extensive than anything done before. This methodology is different from that of the original blast-wave model [7, 37, 38] or the quark recombination model [43]. In addition, differing from the original blast-wave model which studies the kinetic freeze-out temperature and isotropic radial flow, the present work focuses on the kinetic freeze-out temperature and transverse flow which contains together the isotropic radial flow and anisotropic collective flow.

We would like to emphasize that our recent work [31] investigated particularly the methodology based on the analyses of transverse momentum spectra, in which the linear relations between T and m_0, $\langle p_T\rangle$

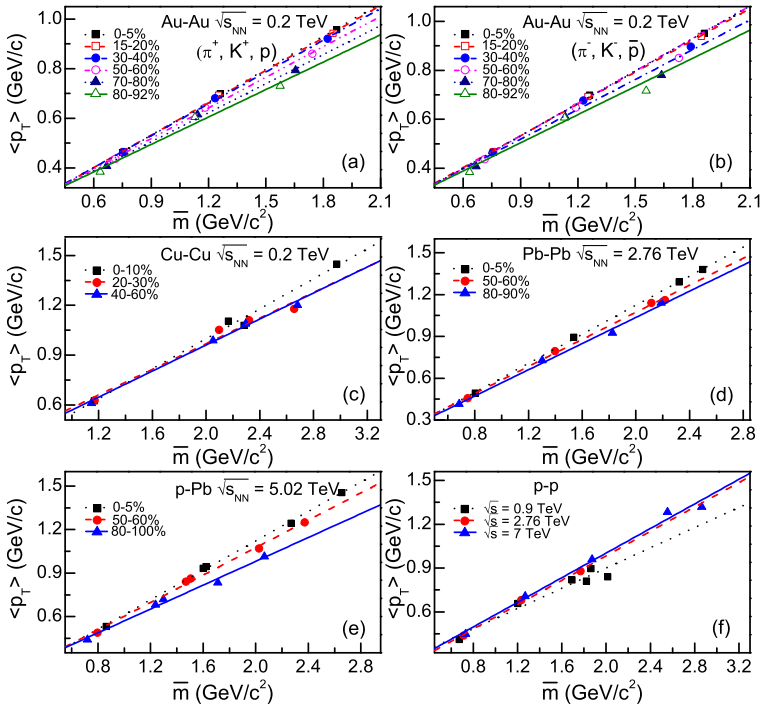

Figure 11. Dependences of $\langle p_T \rangle$ on $\overline{m}$ in (a) 0.2 TeV Au-Au collisions for positive particles, (b) 0.2 TeV Au-Au collisions for negative particles, (c) 0.2 TeV Cu-Cu collisions, (d) 2.76 TeV Pb-Pb collisions, and (e) 5.02 TeV p-Pb collisions with different centralities, as well as (f) p-p collisions at different energies. The symbols are our calculated results due to the parameter values listed in Tables 1 and 2. The lines are our fitted results.

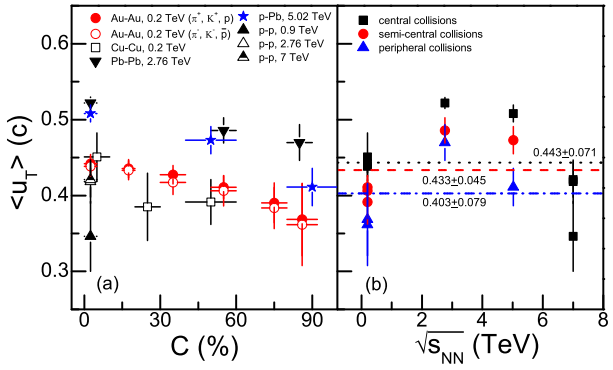

Figure 12. Dependences of $\langle u_T \rangle$ on (a) centrality and (b) energy for different collisions marked in the panel. The symbols are the slopes in Fig. 11. The dotted, dashed, and dotted-dashed lines in Fig. 12(b) are the mean $\langle u_T \rangle$ over energy for central, semi-central, and peripheral collisions, respectively.

and m_0, $\langle p\rangle$ and m_0, T and $\overline{m}$, $\langle p_T\rangle$ and $\overline{m}$, as well as $\langle p\rangle$ and $\overline{m}$ are studied. At the same time, the relations among some intercepts and slopes are studied. The present work focuses on an application of the above methodology. Different kinetic freeze-out temperatures are obtained due to different types of "thermometers" or "thermometric scales" and the same transverse flow velocity is obtained due to the same transverse momentum spectrum. Our descriptions on different "thermometers" or "thermometric scales" can be compared with those in thermodynamics.

In addition, the other difference is that in our recent work [31], the Tsallis distribution and a one- or two-component Erlang distribution is used, while in the present work, the Tsallis-standard, Tsallis, and two- or three-component standard distributions are used. The differences in the description of particle spectra with the three different distributions are marginal and only visible in a few cases at high momentum. This is also reflected in the similar values of the χ^2/dof as listed in Tables 1 and 2 of the present work. In our opinion, among different types of "thermometers" or "thermometric scales", the standard distribution and its multi-component distribution can be used to extract the standard temperature which is closest to the thermodynamic temperature in thermal physics. The other "thermometers" can be regarded as non-standard "thermometers" which can be corrected if necessary.

4 Conclusions

We summarize here our main observations and conclusions.

(a) The transverse momentum spectra of final-state light flavour particles ($\pi^{\pm}$, $K^{\pm}$, K^0_S, p, $\bar{p}$, ϕ, Λ, $\bar{\Lambda}$, Ξ, and Ω, etc.), produced in Au-Au, Cu-Cu, Pb-Pb, p-Pb, and p-p collisions over an energy range from 0.2 to 7 TeV, are described by the Tsallis-standard, Tsallis, and two- or three-component standard distributions which are used in the multisource thermal model as different types of "thermometers" or "thermometric scales" and "speedometers". The characteristic of multiple temperatures in multi-component standard distribution can be described by the Tsallis-standard and Tsallis distributions. The calculated results are in agreement with the experimental data recorded by the PHENIX, STAR, ALICE, and CMS Collaborations. Based on the three types of "thermometers" or "thermometric scales" and "speedometers", the effective temperatures ($T_{\rm T\text{-}S}$, $T_{\rm T}$, and $T_{\rm S}$) and kinetic freeze-out temperatures ($T_{\rm T\text{-}S0}$, $T_{\rm T0}$, and $T_{\rm S0}$) of interacting system at the stage of kinetic freeze-out, and the mean transverse flow velocity of final-state particles are successively extracted from the transverse momentum spectra.

(b) In the extraction of the kinetic freeze-out temperature and transverse flow velocity from the transverse momentum spectra, the methodology used in the present work is different from that of the original blast-wave model with the Boltzmann-Gibbs distribution or the Tsallis statistics, or the quark recombination model with the Cooper-Frye formula and flow. The effect of transverse flow is not directly considered in formulas describing the transverse momentum spectra. Instead, we obtain the effective temperature from the formulas, the kinetic freeze-out temperature from the intercept by plotting the effective temperature versus the particle's rest mass, and the transverse flow velocity from the slope by plotting the mean transverse momentum versus the mean moving mass. Our treatment disentangles naturally the random thermal motion of particles and collective expansion of sources.

(c) The present work shows that the effective temperatures $T_{\rm T\text{-}S}$, $T_{\rm T}$, and $T_{\rm S}$ increase with the increase of centrality or particle's rest mass, and satisfy the relationship $T_{\rm T\text{-}S} \leq T_{\rm T} < T_{\rm S}$ for a given set of data. In most cases, we have $T_{\rm T\text{-}S0} \leq T_{\rm T0} < T_{\rm S0}$. The kinetic freeze-out temperatures decrease slightly with the decrease of centrality, and do not show an obvious change with energy and size for the central, semi-central, and peripheral collisions. The mean kinetic freeze-out temperatures derived from the three types of "thermometers" show $\langle T_{\rm T\text{-}S0}\rangle \leq \langle T_{\rm T0}\rangle < \langle T_{\rm S0}\rangle$, and $\langle T_0\rangle_{\rm central} > \langle T_0\rangle_{\rm semi\text{-}central} \geq \langle T_0\rangle_{\rm peripheral}$. The independences of kinetic freeze-out temperatures on energy and size reveal that different interacting systems at the stage of kinetic freeze-out reached the same excitation degree of hadronic matter in the considered energy range. Generally, the effective temperature is greater than kinetic freeze-out temperature, since the former containing both the thermal motion and flow effect while the latter containing only the thermal motion.

(d) The present work also shows that the central collisions have a higher kinetic freeze-out temperature than that of peripheral collisions. This is consistent with those of the chemical freeze-out temperature and effective temperature. Based on the three temperatures we conclude that the excitation degree of central collisions is higher than that of peripheral collisions at both the chemical and kinetic freeze-out stages. In addition, at the stage of kinetic freeze-out, the transverse flow velocity in central collisions is larger than that in peripheral collisions, indicating a larger squeeze and expansion in central collisions

which also show a higher temperature and excitation degree. Thus, the kinetic freeze-out temperatures, which describe the random thermal motions of particles, and the transverse flow velocities, which describe the collective expansions of sources, paint a consistent picture.

(e) The present work is an application of our recent work [31] in which an alternative method is investigated to extract separately the kinetic freeze-out temperature and flow velocity. If we regard the standard distribution and its multi-component distribution as the most exact and standard "thermometer" due to they being closest to the thermodynamic temperature in thermal physics, we obtain a kinetic freeze-out temperature [(156 ± 6) MeV in central collisions] which is equal to the chemical freeze-out temperature extracted from particle ratios [36]. This indicates that the two freeze-outs had happened at almost the same time even at the RHIC and LHC energies. We would like to treat other two "thermometers" used in the present work as non-standard "thermometers", which can be corrected if necessary. Another application [32] of our alternative method shows an evidence of mass-dependent differential kinetic freeze-out scenario, while the single and double kinetic freeze-out scenarios are eliminated.

(f) In central collisions, the transverse flow mainly contains the isotropic radial flow, since the effect of anisotropic collective flow is small and can be neglected in the extraction of transverse flow which contains mainly the isotropic radial flow. In contrast, the transverse flow of peripheral collisions includes mainly the anisotropic collective flow, since the radial flow is nearly zero. In this work, the transverse flow contains both the isotropic radial flow and anisotropic collective flow, which outperforms the original blast-wave model since it only includes the radial flow. We also found that the radial flow in central collisions is greater than anisotropic collective flow in peripheral collisions.

Acknowledgments

This work was supported by the National Natural Science Foundation of China under Grant No. 11575103 and the US DOE under contract DE-FG02-87ER40331.A008.

References

[1] Gupta N 2008 *A Study of fluctuations in multiplicity distributions at ultra-relativistic heavy ion interactions*, Ph.D. Thesis, University of Jammu, India, https://www.bnl.gov/userscenter/Thesis/2009/ngupta_thesis.pdf.

[2] Meng C-R 2009 *Chin. Phys. Lett.* **26** 102501.

[3] Liu F-H, Gao Y-Q and Wei H R 2014 *Adv. High Energy Phys.* **2014** 293873.

[4] Gao Y-Q, Tian C-X, Duan M-Y, Li B-C and Liu F-H 2012 *Pramana – J. Phys.* **79** 1407.

[5] Wilk G and Wldarczyk Z 2000 *Phys. Rev. Lett.* **84** 2770.

[6] Adams J *et al.* (STAR Collaboration) 2005 *Phys. Rev.* C **71** 064902.

[7] Schnedermann E, Sollfrank J and Heinz U 1993 *Phys. Rev.* C **48** 2462.

[8] Liu F-H 2004 *Phys. Lett.* B **583** 68.

[9] Liu F-H 2008 *Phys. Rev.* C **78** 014902.

[10] Liu F-H 2008 *Nucl. Phys.* A **810** 159.

[11] Adler S S *et al.* (PHENIX Collaboration) 2004 *Phys. Rev.* C **69** 034909.

[12] Agakishiev G *et al.* (STAR Collaboration) 2012 *Phys. Rev. Lett.* **108** 072301.

[13] Abelev B *et al.* (ALICE Collaboration) 2013 *Phys. Rev.* C **88** 044910.

[14] Abelev B *et al.* (ALICE Collaboration) 2015 *Phys. Rev.* C **91** 024609.

[15] Abelev B *et al.* (ALICE Collaboration) 2014 *Phys. Lett.* B **728** 25.

[16] Aamodt K *et al.* (ALICE Collaboration) 2011 *Eur. Phys. J.* C **71** 1594.

[17] Floris M *et al.* (ALICE Collaboration) 2011 *J. Phys.* G **38** 124025.

[18] Adam J *et al.* (ALICE Collaboration) 2015 *Eur. Phys. J.* C **75** 226.

[19] Chatrchyan S *et al.* (CMS Collaboration) 2012 *Eur. Phys. J.* C **72** 2164.

[20] Cleymans J and Worku D 2012 *Eur. Phys. J.* A **48** 160.

[21] Biró T S 2009 *Eur. Phys. J.* A **40** 255.

[22] Biró T S, Purcsel G and Ürmössy K 2009 *Eur. Phys. J.* A **40** 325.

[23] Tsallis C 1988 *J. Stat. Phys.* **52** 479.

[24] Tsallis C 2009 *Braz. J. Phys.* **39** 337.

[25] Biró T S 2001 *Physica* A **300** 424.

[26] Biró T S, Barnaföldi G G, Ván P and Ürmössy K 2014 arXiv:1404.1256 [hep-ph].

[27] Takeuchi S, Murase K, Hirano T, Huovinen P and Nara Y 2015 *Phys. Rev.* C **92** 044907.

[28] Heiselberg H and Levy A M 1999 *Phys. Rev.* C **59** 2716.

[29] Heinz U W 2004 arXiv:hep-ph/0407360.

[30] Russo R 2015 *Measurement of D^+ meson production in p-Pb collisions with the ALICE detector*, Ph.D. Thesis, Universitaâ degli Studi di Torino, Italy, arXiv:1511.04380 [nucl-ex].

[31] Wei H-R, Liu F-H and Lacey R A 2016 *Eur. Phys. J.* A **52** 102.

[32] Lao H-L, Wei H-R, Liu F-H and Lacey R A 2016 *Eur. Phys. J.* A **52** 203.

[33] Fodor Z and Katz S D 2004 *JHEP* **0404** 050.

[34] Datta S, Gavai R V and Gupta S 2013 *Nucl. Phys.* A **904-905** 883c.

[35] Xu N (for the STAR Collaboration) 2014 *Nucl. Phys.* A **931** 1.

[36] Stachel J, Andronic A, Braun-Munzinger P and Redlich K 2014 *J. Phys.* Conf. Ser. **509** 012019.

[37] Tang Z B, Xu Y C, Ruan L J, van Buren G, Wang F Q and Xu Z B 2009 *Phys. Rev.* C **79**, 051901(R).

[38] Shao M, Yi L, Tang Z B, Chen H F, Li C and Xu Z B 2010 *J. Phys.* G **37** 085104.

[39] Shi S S (for the STAR Collaboration) 2016 *J. Phys.* Conf. Ser. **668** 012079.

[40] Huovinen P, Kolb P F, Heinz U, Ruuskanen P V and Voloshin S 2001 *Phys. Lett.* B **503** 58.

[41] Adler C *et al.* (STAR Collaboration) 2001 *Phys. Rev. Lett.* **87** 182301.

[42] Sun X, Masui H, Poskanzer A M and Schmah A 2015 *Phys. Rev.* C **91** 024903.

[43] Ürmössy K and Biró T S 2010 *Phys. Lett.* B **689** 14.

Table 1. Values of free parameters, normalization constants, and χ^2/dof corresponding to Tsallis-standard and Tsallis distributions in Figs. 1–5. The values of χ^2/dof for $\Xi^- + \bar{\Xi}^+$ in Fig. 5(b) are in fact the values of χ^2 values due to less data points. The temperatures are in the units of GeV.

Figure	Type	$T_{\text{T-S}}$	$q_{\text{T-S}}$	$N_{\text{T-S0}}$	χ^2/dof	T_{T}	q_{T}	N_{T0}	χ^2/dof
1(a)	0-5%	0.115 ± 0.003	1.076 ± 0.004	184.342 ± 28.740	0.243	0.120 ± 0.003	1.085 ± 0.005	169.870 ± 25.534	0.311
	15-20%	0.113 ± 0.003	1.080 ± 0.004	109.968 ± 16.776	0.193	0.119 ± 0.003	1.088 ± 0.005	102.208 ± 17.748	0.314
	30-40%	0.108 ± 0.003	1.086 ± 0.004	54.158 ± 8.198	0.347	0.112 ± 0.003	1.097 ± 0.005	52.515 ± 7.948	0.377
	50-60%	0.096 ± 0.003	1.093 ± 0.004	21.693 ± 3.682	0.273	0.103 ± 0.003	1.104 ± 0.006	20.256 ± 3.357	0.324
	70-80%	0.086 ± 0.003	1.097 ± 0.004	5.664 ± 1.114	0.234	0.094 ± 0.003	1.108 ± 0.006	5.234 ± 1.008	0.278
	80-92%	0.078 ± 0.003	1.101 ± 0.005	3.141 ± 0.641	0.149	0.087 ± 0.003	1.112 ± 0.006	2.870 ± 0.584	0.182
1(b)	0-5%	0.119 ± 0.003	1.072 ± 0.004	180.218 ± 26.650	0.190	0.120 ± 0.003	1.085 ± 0.005	169.269 ± 24.783	0.287
	15-20%	0.115 ± 0.003	1.078 ± 0.004	105.190 ± 16.405	0.181	0.113 ± 0.003	1.096 ± 0.005	102.669 ± 15.936	0.188
	30-40%	0.108 ± 0.003	1.086 ± 0.004	53.048 ± 8.028	0.271	0.112 ± 0.003	1.097 ± 0.005	51.420 ± 7.818	0.317
	50-60%	0.096 ± 0.003	1.093 ± 0.004	21.259 ± 3.550	0.220	0.103 ± 0.003	1.104 ± 0.005	19.834 ± 3.249	0.275
	70-80%	0.086 ± 0.003	1.097 ± 0.004	5.542 ± 1.013	0.223	0.094 ± 0.003	1.108 ± 0.005	5.120 ± 0.965	0.264
	80-92%	0.078 ± 0.003	1.101 ± 0.005	3.093 ± 0.641	0.099	0.087 ± 0.003	1.112 ± 0.005	2.826 ± 0.584	0.125
1(c)	0-5%	0.158 ± 0.003	1.066 ± 0.005	19.239 ± 2.343	0.066	0.168 ± 0.003	1.071 ± 0.006	18.916 ± 2.664	0.067
	15-20%	0.155 ± 0.003	1.067 ± 0.004	11.116 ± 1.472	0.023	0.166 ± 0.003	1.072 ± 0.006	10.851 ± 1.426	0.023
	30-40%	0.150 ± 0.003	1.068 ± 0.004	5.383 ± 0.529	0.031	0.160 ± 0.003	1.073 ± 0.006	5.308 ± 0.757	0.032
	50-60%	0.132 ± 0.003	1.074 ± 0.005	1.935 ± 0.350	0.050	0.142 ± 0.003	1.080 ± 0.006	1.914 ± 0.339	0.052
	70-80%	0.117 ± 0.003	1.080 ± 0.006	0.399 ± 0.088	0.132	0.125 ± 0.003	1.088 ± 0.006	0.397 ± 0.082	0.134
	80-92%	0.112 ± 0.003	1.082 ± 0.006	0.197 ± 0.040	0.203	0.121 ± 0.003	1.090 ± 0.006	0.198 ± 0.048	0.201
1(d)	0-5%	0.158 ± 0.003	1.066 ± 0.005	18.146 ± 2.343	0.040	0.168 ± 0.003	1.071 ± 0.006	17.850 ± 2.664	0.034
	15-20%	0.155 ± 0.003	1.067 ± 0.004	10.320 ± 1.472	0.041	0.166 ± 0.003	1.072 ± 0.006	10.067 ± 1.426	0.036
	30-40%	0.150 ± 0.003	1.067 ± 0.004	5.052 ± 0.525	0.030	0.161 ± 0.003	1.072 ± 0.006	4.956 ± 0.514	0.029
	50-60%	0.132 ± 0.003	1.075 ± 0.005	1.784 ± 0.353	0.059	0.144 ± 0.003	1.080 ± 0.006	1.746 ± 0.312	0.062
	70-80%	0.112 ± 0.003	1.083 ± 0.006	0.397 ± 0.076	0.085	0.121 ± 0.003	1.091 ± 0.005	0.379 ± 0.068	0.085
	80-92%	0.108 ± 0.003	1.086 ± 0.006	0.191 ± 0.036	0.178	0.116 ± 0.003	1.095 ± 0.006	0.193 ± 0.042	0.174
1(e)	0-5%	0.250 ± 0.005	1.031 ± 0.005	4.940 ± 0.820	0.295	0.256 ± 0.006	1.032 ± 0.005	5.082 ± 0.847	0.304
	15-20%	0.243 ± 0.005	1.032 ± 0.004	2.929 ± 0.460	0.146	0.252 ± 0.006	1.033 ± 0.004	2.943 ± 0.475	0.150
	30-40%	0.230 ± 0.006	1.035 ± 0.004	1.493 ± 0.302	0.057	0.240 ± 0.005	1.036 ± 0.005	1.492 ± 0.314	0.059
	50-60%	0.197 ± 0.006	1.042 ± 0.004	0.559 ± 0.107	0.049	0.208 ± 0.006	1.043 ± 0.006	0.555 ± 0.104	0.052
	70-80%	0.158 ± 0.004	1.052 ± 0.005	0.126 ± 0.032	0.074	0.168 ± 0.005	1.054 ± 0.005	0.127 ± 0.027	0.076
	80-92%	0.128 ± 0.004	1.058 ± 0.005	0.070 ± 0.023	0.147	0.138 ± 0.005	1.061 ± 0.005	0.069 ± 0.025	0.150
1(f)	0-5%	0.251 ± 0.005	1.029 ± 0.004	3.718 ± 0.715	0.413	0.258 ± 0.006	1.030 ± 0.005	3.771 ± 0.742	0.430
	15-20%	0.245 ± 0.005	1.030 ± 0.004	2.222 ± 0.467	0.231	0.255 ± 0.006	1.030 ± 0.004	2.218 ± 0.490	0.234
	30-40%	0.223 ± 0.006	1.034 ± 0.004	1.161 ± 0.261	0.085	0.233 ± 0.006	1.035 ± 0.005	1.153 ± 0.274	0.082
	50-60%	0.195 ± 0.005	1.041 ± 0.004	0.425 ± 0.093	0.079	0.205 ± 0.006	1.042 ± 0.006	0.426 ± 0.080	0.080
	70-80%	0.158 ± 0.004	1.049 ± 0.005	0.095 ± 0.018	0.119	0.165 ± 0.005	1.052 ± 0.005	0.096 ± 0.024	0.118
	80-92%	0.128 ± 0.004	1.055 ± 0.005	0.057 ± 0.016	0.099	0.138 ± 0.005	1.057 ± 0.005	0.057 ± 0.018	0.097
2(a)	0-10%	0.123 ± 0.007	1.078 ± 0.004	7.085 ± 2.401	0.243	0.132 ± 0.007	1.085 ± 0.004	7.155 ± 2.600	0.242
	20-30%	0.118 ± 0.007	1.080 ± 0.004	3.580 ± 1.194	0.289	0.128 ± 0.007	1.087 ± 0.004	3.504 ± 1.460	0.290
	40-60%	0.115 ± 0.007	1.084 ± 0.004	1.181 ± 0.450	0.196	0.125 ± 0.007	1.092 ± 0.004	1.148 ± 0.546	0.195
2(b)	0-10%	0.219 ± 0.007	1.033 ± 0.004	1.624 ± 0.722	0.786	0.227 ± 0.007	1.034 ± 0.004	1.620 ± 0.733	0.789
	20-30%	0.193 ± 0.007	1.042 ± 0.003	0.778 ± 0.303	0.280	0.198 ± 0.007	1.045 ± 0.004	0.801 ± 0.280	0.275
	40-60%	0.157 ± 0.006	1.054 ± 0.003	0.278 ± 0.104	0.324	0.172 ± 0.006	1.055 ± 0.004	0.270 ± 0.104	0.331
2(c)	0-10%	0.238 ± 0.007	1.031 ± 0.003	0.166 ± 0.050	0.165	0.243 ± 0.006	1.033 ± 0.003	0.167 ± 0.048	0.167
	20-30%	0.221 ± 0.007	1.039 ± 0.003	0.067 ± 0.024	0.382	0.228 ± 0.006	1.042 ± 0.004	0.065 ± 0.023	0.379
	40-60%	0.205 ± 0.007	0.040 ± 0.003	0.022 ± 0.009	0.295	0.210 ± 0.006	1.043 ± 0.003	0.022 ± 0.008	0.343
2(d)	0-10%	0.299 ± 0.007	1.028 ± 0.004	0.032 ± 0.009	0.856	0.306 ± 0.007	1.029 ± 0.005	0.032 ± 0.009	0.858
	20-30%	0.227 ± 0.007	1.041 ± 0.004	0.015 ± 0.003	0.092	0.233 ± 0.007	1.044 ± 0.004	0.016 ± 0.004	0.089
	40-60%	0.215 ± 0.007	1.045 ± 0.004	0.003 ± 0.001	0.081	0.223 ± 0.007	1.048 ± 0.004	0.003 ± 0.001	0.080

Table 1. Continued.

3(a)	0-5%	0.101 ± 0.002	1.112 ± 0.004	467.262 ± 112.560	0.163	0.112 ± 0.002	1.126 ± 0.005	430.964 ± 121.590	0.211
	50-60%	0.085 ± 0.002	1.124 ± 0.004	49.274 ± 11.070	0.123	0.091 ± 0.002	1.147 ± 0.005	48.274 ± 10.284	0.161
	80-90%	0.068 ± 0.002	1.135 ± 0.004	5.142 ± 1.318	0.059	0.071 ± 0.002	1.163 ± 0.005	5.183 ± 0.952	0.114
3(b)	0-5%	0.247 ± 0.003	1.040 ± 0.004	35.583 ± 5.534	0.012	0.258 ± 0.005	1.038 ± 0.005	34.752 ± 5.111	0.009
	50-60%	0.152 ± 0.003	1.092 ± 0.004	3.822 ± 0.665	0.015	0.160 ± 0.004	1.107 ± 0.005	3.822 ± 0.637	0.019
	80-90%	0.118 ± 0.003	1.106 ± 0.004	0.350 ± 0.078	0.055	0.125 ± 0.004	1.123 ± 0.005	0.346 ± 0.077	0.048
3(c)	0-5%	0.368 ± 0.005	1.023 ± 0.005	7.228 ± 1.943	0.319	0.380 ± 0.010	1.023 ± 0.010	7.346 ± 1.920	0.362
	50-60%	0.290 ± 0.005	1.037 ± 0.003	0.867 ± 0.191	0.038	0.305 ± 0.006	1.037 ± 0.005	0.874 ± 0.204	0.041
	80-90%	0.195 ± 0.005	1.058 ± 0.004	0.100 ± 0.029	0.122	0.200 ± 0.005	1.064 ± 0.005	0.104 ± 0.025	0.104
3(d)	0-5%	0.370 ± 0.005	1.026 ± 0.005	13.520 ± 2.914	0.241	0.379 ± 0.007	1.026 ± 0.005	13.487 ± 2.810	0.223
	50-60%	0.340 ± 0.007	1.037 ± 0.005	1.419 ± 0.229	0.294	0.350 ± 0.007	1.040 ± 0.007	1.400 ± 0.262	0.302
	80-90%	0.250 ± 0.007	1.067 ± 0.005	0.094 ± 0.026	0.204	0.256 ± 0.007	1.075 ± 0.007	0.096 ± 0.021	0.182
4(a)	0-5%	0.090 ± 0.003	1.137 ± 0.004	24.935 ± 5.456	0.276	0.099 ± 0.003	1.163 ± 0.005	23.932 ± 5.400	0.371
	40-60%	0.081 ± 0.003	1.137 ± 0.004	10.100 ± 2.104	0.249	0.088 ± 0.003	1.163 ± 0.006	10.008 ± 2.045	0.304
	80-100%	0.064 ± 0.002	1.139 ± 0.004	3.449 ± 0.725	0.008	0.072 ± 0.003	1.164 ± 0.006	3.338 ± 0.747	0.014
4(b)	0-5%	0.273 ± 0.008	1.065 ± 0.005	0.507 ± 0.117	0.107	0.295 ± 0.009	1.068 ± 0.008	0.515 ± 0.124	0.102
	40-60%	0.174 ± 0.005	1.088 ± 0.004	0.234 ± 0.056	0.026	0.184 ± 0.006	1.100 ± 0.007	0.237 ± 0.057	0.032
	80-100%	0.082 ± 0.004	1.107 ± 0.004	0.078 ± 0.022	0.019	0.091 ± 0.004	1.120 ± 0.005	0.079 ± 0.022	0.018
4(c)	0-5%	0.163 ± 0.003	1.112 ± 0.003	1.901 ± 0.242	0.008	0.177 ± 0.003	1.129 ± 0.005	1.915 ± 0.231	0.007
	40-60%	0.130 ± 0.003	1.118 ± 0.003	0.739 ± 0.098	0.009	0.144 ± 0.003	1.135 ± 0.005	0.750 ± 0.094	0.010
	80-100%	0.078 ± 0.002	1.133 ± 0.003	0.234 ± 0.028	0.032	0.090 ± 0.002	1.152 ± 0.005	0.235 ± 0.033	0.031
4(d)	0-5%	0.286 ± 0.005	1.066 ± 0.003	0.346 ± 0.087	0.025	0.301 ± 0.005	1.072 ± 0.004	0.348 ± 0.083	0.025
	40-60%	0.186 ± 0.004	1.087 ± 0.003	0.142 ± 0.034	0.023	0.196 ± 0.005	1.098 ± 0.004	0.144 ± 0.032	0.018
	80-100%	0.091 ± 0.003	1.106 ± 0.003	0.039 ± 0.011	0.025	0.100 ± 0.003	1.119 ± 0.003	0.040 ± 0.013	0.026
4(e)	0-5%	0.165 ± 0.004	1.108 ± 0.003	0.934 ± 0.243	0.002	0.179 ± 0.004	1.123 ± 0.004	0.945 ± 0.212	0.005
	40-60%	0.130 ± 0.003	1.119 ± 0.003	0.372 ± 0.091	0.016	0.145 ± 0.004	1.137 ± 0.004	0.363 ± 0.085	0.026
	80-100%	0.080 ± 0.003	1.133 ± 0.003	0.116 ± 0.030	0.015	0.091 ± 0.003	1.154 ± 0.003	0.117 ± 0.028	0.016
5(a)	π^+	0.084 ± 0.003	1.112 ± 0.006	1.862 ± 0.317	0.055	0.092 ± 0.003	1.127 ± 0.007	1.852 ± 0.308	0.077
	K^+	0.110 ± 0.004	1.097 ± 0.007	0.230 ± 0.029	0.014	0.122 ± 0.004	1.107 ± 0.007	0.229 ± 0.029	0.017
	p	0.148 ± 0.004	1.065 ± 0.005	0.103 ± 0.015	0.085	0.159 ± 0.004	1.069 ± 0.007	0.103 ± 0.015	0.084
5(b)	Λ	0.166 ± 0.003	1.060 ± 0.002	0.046 ± 0.005	1.189	0.175 ± 0.003	1.064 ± 0.002	0.045 ± 0.005	1.192
	ϕ	0.164 ± 0.003	1.081 ± 0.002	0.017 ± 0.002	0.861	0.174 ± 0.003	1.092 ± 0.002	0.018 ± 0.002	0.804
	$\Xi^- + \bar{\Xi}^+$	0.175 ± 0.003	1.055 ± 0.002	0.012 ± 0.002	(0.357)	0.180 ± 0.003	1.060 ± 0.004	0.012 ± 0.002	(0.348)
5(c)	π^+	0.084 ± 0.003	1.121 ± 0.006	2.315 ± 0.382	0.106	0.092 ± 0.003	1.140 ± 0.007	2.305 ± 0.360	0.131
	K^+	0.112 ± 0.003	1.107 ± 0.006	0.298 ± 0.036	0.009	0.123 ± 0.003	1.121 ± 0.008	0.302 ± 0.040	0.014
	p	0.148 ± 0.003	1.076 ± 0.006	0.133 ± 0.019	0.080	0.159 ± 0.003	1.082 ± 0.007	0.134 ± 0.021	0.081
5(d)	π^+	0.080 ± 0.002	1.130 ± 0.004	2.918 ± 0.320	0.100	0.090 ± 0.003	1.150 ± 0.005	2.920 ± 0.319	0.143
	K^+	0.115 ± 0.002	1.110 ± 0.004	0.367 ± 0.030	0.014	0.127 ± 0.003	1.124 ± 0.005	0.376 ± 0.036	0.022
	p	0.148 ± 0.002	1.089 ± 0.003	0.168 ± 0.016	0.044	0.163 ± 0.003	1.098 ± 0.005	0.168 ± 0.016	0.042
5(e)	Ξ	0.179 ± 0.003	1.088 ± 0.002	$(2.356 \pm 0.416) \times 10^{-3}$	0.587	0.188 ± 0.003	1.099 ± 0.002	$(2.389 \pm 0.342) \times 10^{-3}$	0.583
	Ω	0.202 ± 0.003	1.086 ± 0.002	$(2.190 \pm 0.281) \times 10^{-4}$	0.045	0.215 ± 0.003	1.096 ± 0.003	$(2.180 \pm 0.322) \times 10^{-4}$	0.037
5(f)	$\pi^+ + \pi^-$	0.063 ± 0.002	1.148 ± 0.004	4.490 ± 0.726	0.048	0.073 ± 0.002	1.173 ± 0.005	4.484 ± 0.784	0.070
	$K^+ + K^-$	0.095 ± 0.002	1.132 ± 0.003	0.571 ± 0.090	0.017	0.107 ± 0.003	1.153 ± 0.004	0.570 ± 0.099	0.021
	$p + \bar{p}$	0.125 ± 0.002	1.097 ± 0.002	0.240 ± 0.034	0.056	0.137 ± 0.003	1.108 ± 0.003	0.242 ± 0.033	0.050

Table 2. Values of free parameters, $T_{\rm S}$, normalization constant, and χ^2/dof corresponding to two- or three-component standard distributions in Figs. 1–5. The values of χ^2/dof for ϕ and $\Xi^- + \bar{\Xi}^+$ in Fig. 5(b) are the values of χ^2 values due to less data points. The temperatures are in the units of GeV.

Figure	Type	T_1	k_1	T_2	k_2	T_3	$T_{\rm S}$	$N_{\rm S0}$	χ^2/dof
1(a)	0-5%	0.139 ± 0.010	0.874 ± 0.020	0.276 ± 0.010	-	-	0.156 ± 0.010	193.000 ± 30.000	0.306
	15-20%	0.142 ± 0.010	0.896 ± 0.020	0.298 ± 0.010	-	-	0.158 ± 0.010	109.000 ± 15.000	0.293
	30-40%	0.142 ± 0.010	0.913 ± 0.010	0.309 ± 0.010	-	-	0.156 ± 0.010	54.500 ± 8.000	0.457
	50-60%	0.137 ± 0.008	0.929 ± 0.010	0.315 ± 0.010	-	-	0.150 ± 0.008	20.500 ± 3.000	0.449
	70-80%	0.130 ± 0.010	0.935 ± 0.010	0.305 ± 0.010	-	-	0.141 ± 0.010	5.110 ± 0.800	0.344
	80-92%	0.121 ± 0.010	0.932 ± 0.010	0.291 ± 0.010	-	-	0.132 ± 0.010	2.800 ± 0.400	0.237
1(b)	0-5%	0.140 ± 0.010	0.860 ± 0.020	0.271 ± 0.010	-	-	0.158 ± 0.010	188.000 ± 28.000	0.269
	15-20%	0.145 ± 0.010	0.891 ± 0.020	0.293 ± 0.010	-	-	0.161 ± 0.010	102.000 ± 13.000	0.335
	30-40%	0.143 ± 0.008	0.913 ± 0.010	0.309 ± 0.010	-	-	0.157 ± 0.008	52.800 ± 7.000	0.483
	50-60%	0.140 ± 0.010	0.926 ± 0.010	0.315 ± 0.010	-	-	0.153 ± 0.009	19.320 ± 2.000	0.495
	70-80%	0.129 ± 0.009	0.926 ± 0.010	0.301 ± 0.010	-	-	0.142 ± 0.008	4.910 ± 0.800	0.354
	80-92%	0.122 ± 0.010	0.929 ± 0.015	0.291 ± 0.020	-	-	0.134 ± 0.010	2.700 ± 0.500	0.245
1(c)	0-5%	0.207 ± 0.010	0.871 ± 0.030	0.390 ± 0.030	-	-	0.231 ± 0.011	18.400 ± 2.000	0.062
	15-20%	0.206 ± 0.010	0.866 ± 0.030	0.382 ± 0.030	-	-	0.230 ± 0.011	10.400 ± 1.000	0.026
	30-40%	0.202 ± 0.010	0.878 ± 0.030	0.385 ± 0.030	-	-	0.224 ± 0.011	5.060 ± 0.500	0.040
	50-60%	0.191 ± 0.010	0.887 ± 0.030	0.362 ± 0.030	-	-	0.210 ± 0.011	1.810 ± 0.200	0.093
	70-80%	0.169 ± 0.010	0.845 ± 0.030	0.325 ± 0.025	-	-	0.193 ± 0.010	0.389 ± 0.080	0.142
	80-92%	0.165 ± 0.015	0.840 ± 0.030	0.320 ± 0.030	-	-	0.190 ± 0.014	0.188 ± 0.040	0.200
1(d)	0-5%	0.210 ± 0.010	0.866 ± 0.030	0.384 ± 0.030	-	-	0.233 ± 0.011	16.800 ± 2.000	0.025
	15-20%	0.220 ± 0.010	0.912 ± 0.030	0.410 ± 0.030	-	-	0.237 ± 0.011	9.170 ± 1.000	0.055
	30-40%	0.202 ± 0.010	0.878 ± 0.030	0.385 ± 0.030	-	-	0.224 ± 0.011	4.710 ± 0.500	0.038
	50-60%	0.191 ± 0.010	0.877 ± 0.030	0.362 ± 0.020	-	-	0.212 ± 0.010	1.650 ± 0.200	0.074
	70-80%	0.169 ± 0.010	0.855 ± 0.030	0.330 ± 0.025	-	-	0.192 ± 0.010	0.378 ± 0.080	0.098
	80-92%	0.165 ± 0.015	0.840 ± 0.040	0.320 ± 0.030	-	-	0.190 ± 0.018	0.182 ± 0.040	0.184
1(e)	0-5%	0.310 ± 0.010	0.980 ± 0.020	0.520 ± 0.030	-	-	0.314 ± 0.011	4.500 ± 1.000	0.216
	15-20%	0.300 ± 0.020	0.900 ± 0.030	0.420 ± 0.030	-	-	0.312 ± 0.019	2.600 ± 0.600	0.166
	30-40%	0.264 ± 0.020	0.900 ± 0.030	0.427 ± 0.020	-	-	0.280 ± 0.018	1.500 ± 0.200	0.061
	50-60%	0.240 ± 0.020	0.900 ± 0.030	0.400 ± 0.030	-	-	0.256 ± 0.019	0.560 ± 0.100	0.040
	70-80%	0.205 ± 0.020	0.920 ± 0.030	0.400 ± 0.030	-	-	0.221 ± 0.019	0.135 ± 0.020	0.032
	80-92%	0.180 ± 0.030	0.920 ± 0.040	0.360 ± 0.030	-	-	0.194 ± 0.029	0.076 ± 0.015	0.117
1(f)	0-5%	0.300 ± 0.020	0.970 ± 0.020	0.490 ± 0.030	-	-	0.306 ± 0.020	3.500 ± 0.800	0.283
	15-20%	0.300 ± 0.020	0.970 ± 0.020	0.480 ± 0.030	-	-	0.305 ± 0.020	2.000 ± 0.400	0.155
	30-40%	0.265 ± 0.020	0.910 ± 0.030	0.410 ± 0.030	-	-	0.278 ± 0.019	1.100 ± 0.200	0.070
	50-60%	0.240 ± 0.020	0.910 ± 0.030	0.400 ± 0.030	-	-	0.254 ± 0.019	0.430 ± 0.100	0.059
	70-80%	0.205 ± 0.020	0.890 ± 0.030	0.360 ± 0.020	-	-	0.222 ± 0.018	0.100 ± 0.030	0.109
	80-92%	0.180 ± 0.020	0.810 ± 0.050	0.300 ± 0.030	-	-	0.203 ± 0.018	0.056 ± 0.015	0.104
2(a)	0-10%	0.230 ± 0.040	0.881 ± 0.001	0.350 ± 0.040	0.117 ± 0.001	0.660 ± 0.030	0.245 ± 0.036	4.500 ± 2.000	0.490
	20-30%	0.217 ± 0.050	0.788 ± 0.002	0.315 ± 0.040	0.208 ± 0.001	0.624 ± 0.030	0.239 ± 0.040	2.100 ± 0.900	0.328
	40-60%	0.195 ± 0.050	0.792 ± 0.001	0.321 ± 0.040	0.205 ± 0.001	0.650 ± 0.030	0.222 ± 0.040	0.870 ± 0.300	0.206
2(b)	0-10%	0.305 ± 0.020	0.960 ± 0.003	0.360 ± 0.030	0.035 ± 0.003	0.550 ± 0.030	0.308 ± 0.021	1.250 ± 0.300	0.441
	20-30%	0.270 ± 0.020	0.932 ± 0.003	0.390 ± 0.030	0.060 ± 0.003	0.510 ± 0.030	0.279 ± 0.020	0.700 ± 0.200	0.208
	40-60%	0.260 ± 0.030	0.950 ± 0.003	0.400 ± 0.030	0.040 ± 0.004	0.500 ± 0.030	0.268 ± 0.030	0.250 ± 0.100	0.350
2(c)	0-10%	0.310 ± 0.020	0.950 ± 0.020	0.465 ± 0.020	-	-	0.317 ± 0.019	0.150 ± 0.050	0.224
	20-30%	0.310 ± 0.020	0.950 ± 0.020	0.490 ± 0.020	-	-	0.319 ± 0.019	0.057 ± 0.015	0.336
	40-60%	0.295 ± 0.020	0.950 ± 0.020	0.470 ± 0.020	-	-	0.304 ± 0.019	0.019 ± 0.005	0.324
2(d)	0-10%	0.378 ± 0.020	0.990 ± 0.010	0.610 ± 0.050	-	-	0.380 ± 0.019	0.030 ± 0.010	1.170
	20-30%	0.316 ± 0.030	0.940 ± 0.020	0.550 ± 0.050	-	-	0.330 ± 0.029	0.015 ± 0.005	0.226
	40-60%	0.308 ± 0.030	0.900 ± 0.030	0.513 ± 0.050	-	-	0.328 ± 0.028	0.003 ± 0.001	0.203

Table 2. Continued.

3(a)	0-5%	0.094 ± 0.020	0.650 ± 0.005	0.254 ± 0.020	0.341 ± 0.005	0.530 ± 0.060	0.152 ± 0.030	510.000 ± 100.000	0.025
	50-60%	0.083 ± 0.020	0.642 ± 0.005	0.208 ± 0.020	0.325 ± 0.005	0.413 ± 0.020	0.134 ± 0.024	57.000 ± 10.000	0.028
	80-90%	0.078 ± 0.020	0.635 ± 0.005	0.195 ± 0.020	0.342 ± 0.005	0.430 ± 0.020	0.126 ± 0.026	5.500 ± 1.000	0.021
3(b)	0-5%	0.275 ± 0.020	0.750 ± 0.030	0.389 ± 0.020	-	-	0.304 ± 0.016	35.000 ± 5.000	0.009
	50-60%	0.195 ± 0.020	0.680 ± 0.040	0.377 ± 0.015	-	-	0.253 ± 0.016	3.800 ± 0.500	0.019
	80-90%	0.160 ± 0.020	0.725 ± 0.030	0.363 ± 0.015	-	-	0.216 ± 0.016	0.360 ± 0.060	0.048
3(c)	0-5%	0.447 ± 0.020	0.850 ± 0.020	0.300 ± 0.020	-	-	0.425 ± 0.018	6.800 ± 2.000	0.010
	50-60%	0.340 ± 0.020	0.950 ± 0.010	0.600 ± 0.020	-	-	0.353 ± 0.019	0.870 ± 0.150	0.019
	80-90%	0.228 ± 0.020	0.845 ± 0.020	0.440 ± 0.020	-	-	0.261 ± 0.018	0.110 ± 0.020	0.065
3(d)	0-5%	0.430 ± 0.020	0.950 ± 0.030	0.670 ± 0.050	-	-	0.442 ± 0.020	13.500 ± 3.000	0.289
	50-60%	0.370 ± 0.030	0.850 ± 0.030	0.650 ± 0.050	-	-	0.412 ± 0.028	1.470 ± 0.200	0.157
	80-90%	0.290 ± 0.020	0.750 ± 0.030	0.610 ± 0.030	-	-	0.370 ± 0.019	0.100 ± 0.020	0.060
4(a)	0-5%	0.068 ± 0.020	0.560 ± 0.010	0.200 ± 0.020	0.377 ± 0.010	0.430 ± 0.020	0.140 ± 0.014	30.560 ± 7.000	0.024
	40-60%	0.071 ± 0.020	0.625 ± 0.010	0.205 ± 0.020	0.335 ± 0.010	0.443 ± 0.020	0.131 ± 0.015	12.000 ± 3.000	0.037
	80-100%	0.085 ± 0.020	0.632 ± 0.005	0.195 ± 0.015	0.352 ± 0.004	0.478 ± 0.020	0.130 ± 0.030	3.450 ± 0.800	0.049
4(b)	0-5%	0.283 ± 0.050	0.608 ± 0.080	0.510 ± 0.030	-	-	0.372 ± 0.037	0.510 ± 0.100	0.117
	40-60%	0.240 ± 0.050	0.730 ± 0.050	0.480 ± 0.030	-	-	0.305 ± 0.039	0.230 ± 0.050	0.036
	80-100%	0.190 ± 0.030	0.873 ± 0.030	0.445 ± 0.030	-	-	0.222 ± 0.027	0.080 ± 0.020	0.060
4(c)	0-5%	0.196 ± 0.050	0.556 ± 0.080	0.413 ± 0.030	-	-	0.292 ± 0.035	1.900 ± 0.400	0.019
	40-60%	0.175 ± 0.050	0.640 ± 0.080	0.388 ± 0.030	-	-	0.252 ± 0.038	0.750 ± 0.200	0.018
	80-100%	0.150 ± 0.040	0.770 ± 0.070	0.360 ± 0.020	-	-	0.198 ± 0.034	0.240 ± 0.060	0.042
4(d)	0-5%	0.310 ± 0.050	0.590 ± 0.004	0.520 ± 0.030	0.400 ± 0.004	0.982 ± 0.050	0.401 ± 0.032	0.350 ± 0.070	0.085
	40-60%	0.250 ± 0.050	0.540 ± 0.005	0.424 ± 0.030	0.442 ± 0.005	0.842 ± 0.040	0.338 ± 0.030	0.140 ± 0.030	0.094
	80-100%	0.180 ± 0.050	0.563 ± 0.003	0.358 ± 0.030	0.426 ± 0.003	0.800 ± 0.040	0.263 ± 0.031	0.040 ± 0.010	0.147
4(e)	0-5%	0.210 ± 0.050	0.451 ± 0.002	0.370 ± 0.020	0.530 ± 0.002	0.862 ± 0.030	0.307 ± 0.025	0.940 ± 0.200	0.006
	40-60%	0.180 ± 0.050	0.576 ± 0.002	0.348 ± 0.020	0.407 ± 0.002	0.840 ± 0.030	0.260 ± 0.030	0.380 ± 0.070	0.006
	80-100%	0.130 ± 0.040	0.598 ± 0.002	0.305 ± 0.020	0.390 ± 0.002	0.780 ± 0.030	0.206 ± 0.025	0.120 ± 0.020	0.012
5(a)	π^+	0.124 ± 0.010	0.738 ± 0.050	0.285 ± 0.020	-	-	0.166 ± 0.012	1.870 ± 0.200	0.069
	K^+	0.165 ± 0.010	0.610 ± 0.070	0.363 ± 0.040	-	-	0.242 ± 0.022	0.235 ± 0.030	0.030
	p	0.187 ± 0.020	0.637 ± 0.050	0.380 ± 0.040	-	-	0.257 ± 0.022	0.106 ± 0.010	0.027
5(b)	Λ	0.188 ± 0.030	0.610 ± 0.060	0.370 ± 0.020	-	-	0.260 ± 0.023	0.050 ± 0.005	1.431
	ϕ	0.170 ± 0.020	0.600 ± 0.060	0.450 ± 0.020	-	-	0.282 ± 0.022	0.021 ± 0.002	(0.371)
	$\Xi^- + \bar{\Xi}^+$	0.190 ± 0.030	0.730 ± 0.050	0.470 ± 0.030	-	-	0.266 ± 0.030	0.013 ± 0.001	(0.014)
5(c)	π^+	0.122 ± 0.010	0.670 ± 0.050	0.285 ± 0.020	-	-	0.176 ± 0.012	2.300 ± 0.300	0.068
	K^+	0.167 ± 0.020	0.550 ± 0.080	0.368 ± 0.040	-	-	0.257 ± 0.026	0.305 ± 0.040	0.014
	p	0.189 ± 0.030	0.555 ± 0.100	0.400 ± 0.060	-	-	0.283 ± 0.038	0.137 ± 0.020	0.043
5(d)	π^+	0.122 ± 0.010	0.650 ± 0.050	0.296 ± 0.020	-	-	0.183 ± 0.013	2.900 ± 0.300	0.094
	K^+	0.169 ± 0.010	0.540 ± 0.060	0.368 ± 0.040	-	-	0.260 ± 0.022	0.375 ± 0.030	0.019
	p	0.210 ± 0.020	0.510 ± 0.090	0.410 ± 0.050	-	-	0.308 ± 0.032	0.167 ± 0.015	0.043
5(e)	Ξ	0.270 ± 0.040	0.510 ± 0.010	0.470 ± 0.030	0.450 ± 0.010	0.880 ± 0.030	0.384 ± 0.026	$(2.350 \pm 0.300) \times 10^{-3}$	0.733
	Ω	0.340 ± 0.040	0.680 ± 0.050	0.660 ± 0.050	-	-	0.442 ± 0.035	$(2.200 \pm 0.300) \times 10^{-4}$	0.084
5(f)	$\pi^+ + \pi^-$	0.096 ± 0.020	0.584 ± 0.010	0.254 ± 0.020	0.384 ± 0.010	0.650 ± 0.040	0.174 ± 0.016	4.480 ± 0.800	0.061
	$K^+ + K^-$	0.160 ± 0.030	0.550 ± 0.009	0.358 ± 0.020	0.405 ± 0.009	0.800 ± 0.030	0.269 ± 0.020	0.570 ± 0.100	0.021
	$p + \bar{p}$	0.180 ± 0.030	0.548 ± 0.010	0.360 ± 0.020	0.409 ± 0.010	0.689 ± 0.030	0.276 ± 0.019	0.247 ± 0.040	0.009